Experimental Assessment of the Input Dependence of Nonlinear Data-driven Models

Maren Scheel[a], Gleb Kleyman[b], Ali Tatar[c], Matthew R.W. Brake[d], Simon Peter[e], Jean-Philippe Noël[f], Matthew S. Allen[g], Malte Krack[a]

[a]*Institute of Aircraft Propulsion Systems, University of Stuttgart, Pfaffenwaldring 6, 70569 Stuttgart, Germany scheel@ila.uni-stuttgart.de, krack@ila.uni-stuttgart.de*
[b]*Institute of Dynamics and Vibration Research, Leibniz Universität Hannover, Appelstrasse 11, 30167 Hannover, Germany; kleyman@ids.uni-hannover.de*
[c]*Department of Mechanical Engineering, South Kensington Campus, London SW7 2AZ, UK; a.tatar16@imperial.ac.uk*
[d]*Department of Mechanical Engineering, 6100 Main St., 101 Mechanical Engineering Building, Houston, Texas 77005-1827, USA; brake@rice.edu*
[e]*Institute for Nonlinear Mechanics, University of Stuttgart, Pfaffenwaldring 9, 70569 Stuttgart, Germany; peter@inm.uni-stuttgart.de*
[f]*Space Structures and Systems Laboratory (S3L), Department of Aerospace and Mechanical Engineering, University of Liège, 1 Chemin des Chevreuils (B52/3), B-4000 Liège, Belgium; jp.noel@ulg.ac.be*
[g]*Department of Engineering Physics, University of Wisconsin, 1500 Engineering Drive, 535 Engineering Research Building, Madison, WI 53706, USA; msallen@engr.wisc.edu*

Abstract

Arguably one of the major difficulties associated with nonlinear system identification, compared to a linear problem setting, is the inevitable presence of modeling errors. Stated differently, a nonlinear data-driven model is inherently an approximate description of the true system dynamics. For this reason, it is also strongly dependent upon the considered input signal type and parameters. In the present paper, two experimental test rigs, a magnetic cantilever beam and a free-free beam with a lap joint, are identified using two methodologies operating at extreme sides of the input data spectrum. The first methodology focuses on identifying the system using steady-state excitations. To accomplish this, a phase-locked loop controller is implemented to acquire periodic oscillations near resonance and construct models in the form of nonlinear modal features. The second methodology exploits uncontrolled experiments with transient random inputs to build polynomial nonlinear state-space models using advanced system identification tools. The resulting nonlinear modal and state-space models are challenged to predict dynamic behaviors observed under different sine and sine-sweep excitations, clearly highlighting their capabilities and limitations as dictated by the input domain where they were estimated.

Keywords: nonlinear system identification, polynomial nonlinear state-space identification, nonlinear modal analysis, jointed structures, modal testing

1. Introduction

2. Identification of Nonlinear Models

In this section, we explain the input signals for both methods, PNLSS identification and modal testing as well as the identification procedures and the subsequent vibration prediction. We refer the interested reader to the references given below for further details.

2.1. PNLSS model

A PNLSS model is a multiple-input-multiple-output state-space model, with a linear state-space model $(\mathbf{A}, \mathbf{B}, \mathbf{C}, \mathbf{D})$ as basis that is extended by nonlinear basis functions. For both test specimens in this study, the excitation is described

with one input $u \in \mathbb{R}^1$, and the measured response signals are collected in the output vector $\boldsymbol{y} \in \mathbb{R}^l$. The PNLSS model is then

$$\begin{cases} \boldsymbol{x}(t_{k+1}) = \mathbf{A}\boldsymbol{x}(t_k) + \mathbf{B}u(t_k) + \mathbf{E}\boldsymbol{\varepsilon}(\boldsymbol{x}(\mathrm{t_k}), \mathrm{u}(\mathrm{t_k})) \\ \quad \boldsymbol{y}(t_k) = \mathbf{C}\boldsymbol{x}(t_k) + \mathbf{D}u(t_k) + \mathbf{F}\boldsymbol{\chi}(\boldsymbol{x}(\mathrm{t_k}), \mathrm{u}(\mathrm{t_k})). \end{cases} \tag{1}$$

Here, $t_k \in \mathbb{R}_+$ denotes the discrete time at step k, $\boldsymbol{x} \in \mathbb{R}^s$ the state vector, $\mathbf{A} \in \mathbb{R}^{s\times s}$, $\mathbf{B} \in \mathbb{R}^s$, $\mathbf{C} \in \mathbb{R}^{l\times s}$, $\mathbf{D} \in \mathbb{R}^l$ are linear state, input, output and feedthrough matrices. In this work, we follow the excitation and identification procedure described in [5], using the PNLSS MATLAB toolbox [6]. The nonlinear basis functions are polynomials both in the states and inputs. Multivariate polynomials are straightforward to compute and a wide class of nonlinearities can be modeled with them [4]. The monomial combinations of degree 2 up to degree d are listed in $\boldsymbol{\varepsilon} \in \mathbb{R}^{\mathrm{n_e}}$ and $\boldsymbol{\chi} \in \mathbb{R}^{\mathrm{n_f}}$. Their coefficients are gathered in $\mathbf{E} \in \mathbb{R}^{s\times n_e}$ and $\mathbf{F} \in \mathbb{R}^{l\times n_f}$.

If one can classifies the type of nonlinearity in odd or even prior to the identification by exciting with a manipulated multisine signal [5, 7], it is possible to reduce the number of monomials. The multisine signal includes so-called detection lines. By analyzing the response signal and noting which frequency lines are present, one can distinguish between odd and even nonlinearities, associated with odd and even polynomials.

2.1.1. Excitation with Random Input

In this work, we excite the system with a random, broadband signal that covers at least the expected frequency shift due to the nonlinearity. One example of such a signal is a multisine signal with random phases. Multisine signals are a popular choice in system identification because they allow for a user-defined amplitude spectrum and for a leakage-free analysis due to the periodicity. Moreover, using a multisine reduces the effort to setup the experiment since many commercial testing packages have implemented multisine signals. Formally, the multisine is a sum of sine waves with random phases, drawn from a uniform distribution [8],

$$u(t) = \frac{1}{\sqrt{N}} \sum_{k=-N/2+1}^{k=N/2-1} U_k \mathrm{e}^{\mathrm{i}(2\pi k f_s t/N + \varphi_k)}. \tag{2}$$

Here, N is number of time samples, f_s the sampling frequency, i the imaginary unit. Further, it holds that $U_k = U_{-k}$, $U_0 = 0$, and $\varphi_k = -\varphi_{-k}$. The actual excitation signal consists of several repetitions (called blocks) of one realization (see Fig. 1). This way, transients due to initial conditions decay during the first few blocks, which are discarded for the identification. Then, several experiments are conducted to gather training data, each experiment with a different realization.

The excitation amplitude spectrum must be chosen carefully such that the structure's nonlinearity is indeed excited. Theoretically, if the model order is sufficient and the nonlinearity basis functions can replicate the dynamics, the identified model parameters are independent of the excitation level as the parameters are retrieved exactly. This, however, will generally not hold. Therefore, the amplitude level defines the valid regime of the model and the fitted polynomials are only valid around the tested amplitude range. Outside this regime, extrapolation of the polynomial functions gives false results. To enrich the training data, it can be favorable to identify a model based on an input signal that is composed of several excitation levels [9]. Note at this point that we will later predict vibrations under harmonic excitation. However, it is unclear how define a valid regime based on a root mean square (rms) level of a broadband signal to match a harmonic signal amplitude.

2.1.2. Identification

Identifying a PNLSS model is a four-step procedure. First, measured frequency response functions are averaged over all periods and experiments which gives the so-called best linear approximation (BLA) [8]. Second, a linear state-space model $(\mathbf{A}, \mathbf{B}, \mathbf{C}, \mathbf{D})$ is fitted to the BLA using frequency-domain subspace identification [8, 10]. Third, the linear state-space model is improved by nonlinear optimization solved with a Levenberg-Marquardt algorithm. To this end, an error measure e is defined in the frequency domain as the difference of the frequency response matrix of measured data and model at normalized frequencies [6]. The cost function V_L of the optimization problem is the sum of the mean-square errors, weighted with the inverse of the covariance matrix of the measured frequency response

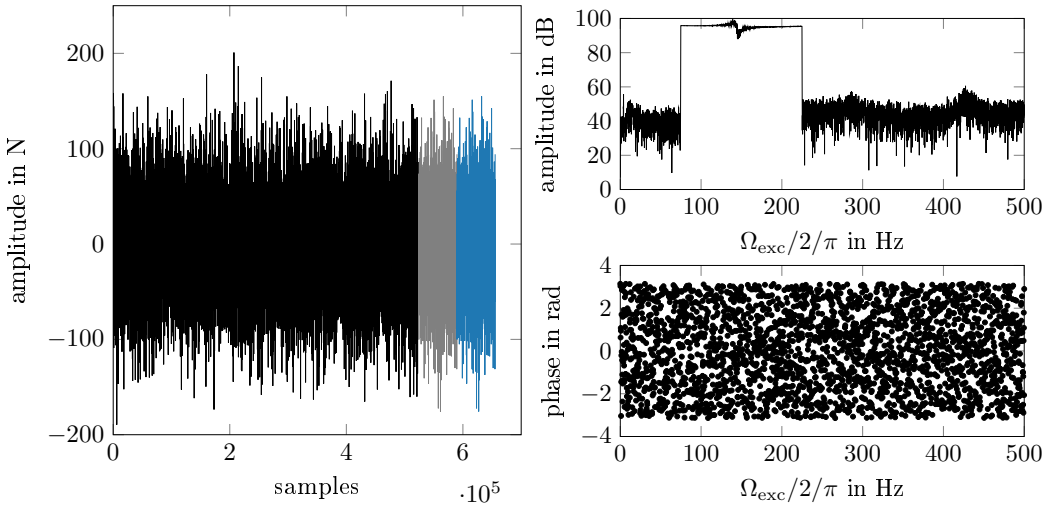

(a) (b)

Figure 1: Multisine signal in (a) time domain and (b) frequency domain. Note that the excitation force amplitude spectrum is not flat due to shaker-structure interactions. Blocks depicted in black are data used in the identification, the block depicted in gray is the validation data set (also part of the identification procedure) and the block depicted in blue is used for testing data.

matrix $\mathbf{G}$,

$$\begin{aligned} &\underset{(\mathbf{A},\mathbf{B},\mathbf{C},\mathbf{D})}{\text{minimize}} \quad V_L \\ &\text{with } e = \mathbf{G} - (\mathbf{C}(z\mathbf{I}-\mathbf{A})^{-1}\mathbf{B}+\mathbf{D}) \\ &\text{and } V_L = e^{\mathrm{T}}\mathrm{cov}(\mathbf{G})^{-1}e. \end{aligned} \tag{3}$$

Here, z is the discrete-time frequency variable that stems from the z-transform and $\mathbf{I}$ is the identity matrix. Finally, the linear model is extended with polynomials. To fit the parameters $(\mathbf{A},\mathbf{B},\mathbf{C},\mathbf{D},\mathbf{E},\mathbf{F})$ to measured data, another nonlinear optimization problem is solved with Levenberg-Marquardt. The initial model for the optimization is the linear state-space model with $\mathbf{E}=\mathbf{F}=\mathbf{0}$. The cost function V_L is the squared difference between the simulated y_{sim} and the measured output y_{ref} in time domain,

$$\begin{aligned} &\underset{(\mathbf{A},\mathbf{B},\mathbf{C},\mathbf{D},\mathbf{E},\mathbf{F})}{\text{minimize}} \quad V_L \\ &\text{with } e = y_{\mathrm{ref}} - y_{\mathrm{sim}} \\ &\text{and } V_L = e^{\mathrm{T}}e. \end{aligned} \tag{4}$$

The initial conditions for input and state in the time simulation of y_{sim} are zero. The first block, which is influenced by transients, is discarded.

2.1.3. Prediction Vibrations

For the prediction of steady-state vibrations, we use the MATLAB tool NLvib for harmonic balance including an alternating time-frequency scheme and path continuation [11]. Harmonic balance for state-space models is explained in [12]. Note that in this work, discrete state-space models are used with the ansatz

$$\boldsymbol{x}_k = \mathrm{Re}\left\{\sum_{k=0}^{H} Q_h \mathrm{e}^{\mathrm{i}h\Omega t_k}\right\} \tag{5}$$

It is important to note at that excitation is assumed to be purely sinusoidal.

For the prediction of transient vibrations, the PNLSS model is evaluated for all time steps, given a known transient input force. Note that the force has to available to the time steps t_k of the discrete state-space model. Therefore, resampling might be necessary if the input force was recorded with a different sampling rate.

2.2. Nonlinear Modal Model

The nonlinear modal analysis conducted in this study is based on the extended periodic motion concept [13]. This concept was introduced for systems described with the differential equation

$$\mathbf{M}\ddot{\boldsymbol{\eta}}(t)+\mathbf{K}\boldsymbol{\eta}(t)+\boldsymbol{g}(\boldsymbol{\eta}(t),\dot{\boldsymbol{\eta}}(t))=\mathbf{0}, \tag{6}$$

with $\boldsymbol{\eta}$ being a vector of generalized coordinates, t the time and $\dot{()}$ the derivative with respect to time. Subsequently, explicit time dependence is dropped for brevity. $\mathbf{M}=\mathbf{M}^{\mathrm{T}}$ and $\mathbf{K}=\mathbf{K}^{\mathrm{T}}$ are the positive definite mass matrix and semi-positive stiffness matrix, respectively. All conservative and nonconservative nonlinear forces as well as linear damping forces are collected in the force vector $\boldsymbol{g}$. Often, forced responses close to primary resonances or self-excited vibrations under negative damping of a certain mode are relevant in technical applications. In these cases, the structure can undergo periodic vibrations. To study these vibrations, the nonlinear mode according to the extended periodic motion concept is defined as a family of periodic motion, $\boldsymbol{\eta}(t)=\boldsymbol{\eta}(t+T)$. However, the damped, autonomous system of Eq. (6) does not vibrate periodically. Therefore, periodic motion has to be enforced by adding an artificial negative damping term $-\xi\mathbf{M}\dot{\boldsymbol{\eta}}$ to the system,

$$\mathbf{M}\ddot{\boldsymbol{\eta}}+\mathbf{K}\boldsymbol{\eta}+\boldsymbol{g}(\boldsymbol{\eta},\dot{\boldsymbol{\eta}})-\xi\mathbf{M}\dot{\boldsymbol{\eta}}=\mathbf{0}. \tag{7}$$

This negative damping term does not intend to cancel all the linear and nonlinear damping forces at every location and every time instant. Instead, the purpose of the artificial term is to compensate the energy dissipated over a period of vibration. The mode according to the extended periodic motion concept is consistent both with the linear normal modes for linear systems under modal damping and with nonlinear modes defined as periodic motion of conservative systems, often referred to as nonlinear normal modes. However, the concept is only valid for isolated resonances. In case of high damping and modal interactions, the negative damping term can cause distortions [13].

2.2.1. Excitation with Controlled Input

To isolate the mode under investigation in an experiment, periodic motion must be excited and the excitation should replicate the negative damping term as closely as possible. To this end, we aim for phase resonance with force appropriation. This approach is taken from [14] where the excitation force is applied only at one location. Phase resonance is achieved when the phase lag between force and vibration response at the excitation location is 90°. This is ensured using a phase controller, called phase-locked loop (PLL), which adapts the excitation frequency until the desired phase lag is reached. The controller is shown schematically in Appendix A. Note that the tuning of the control parameters influence the measurement durations significantly. It is important to note that only the phase lag between the fundamental harmonics of force and response is controlled. Due to shake-structure interactions, uncontrolled higher harmonics can be present. Then, the excitation force $f(t)$ can be written with the Fourier series

$$f(t)=\underbrace{\mathrm{Re}\left\{F_1\mathrm{e}^{\mathrm{i}\Omega t}\right\}}_{\text{fundamental}}+\underbrace{\mathrm{Re}\left\{\sum_{n=2}^{\infty}F_n\mathrm{e}^{\mathrm{i}n\Omega t}\right\}}_{\text{uncontrolled higher harmonics}}. \tag{8}$$

Here, Ω is the excitation frequency which is set by the PLL and is equal to the resonance frequency, $\Omega=\tilde{\omega}$ for phase resonance. F_n with $n\geq 2$ are the amplitudes of the uncontrolled higher harmonics. The amplitude of the fundamental harmonic F_1 can be set by the user. This is therefore possible to change the amplitude during measurement and to follow the backbone curve of the system. In an experiment with shaker-stinger excitation, the user actually sets the amplitude of the voltage input to the power amplifier. The true force amplitude can be measured and is a result of the voltage level and the shaker-structure-interaction.

The excitation force distortion due to higher harmonics is often quantified with the fundamental harmonic content γ [15]. It gives a value between 0 and 1 with 1 for pure sinusoidal signals. Typically, γ decreases for higher amplitudes

where shaker-structure interactions are more dominant. It is possible to determine γ as a function of the vibration level during the nonlinear modal analysis.

2.2.2. Identification

The identified model is a single-degree-of-freedom oscillator that replicates the dynamics around an isolated resonance with the modal properties resonance frequency $\tilde{\omega}$, damping ratio $\tilde{\zeta}$ and deflection shape $\tilde{\boldsymbol{\psi}}$. These properties depend on the vibration level, indicated by the tilde $\tilde{()}$. The resonance frequency $\tilde{\omega}$ as well as the deflection shapes $\tilde{\boldsymbol{\psi}}$ can be extracted directly from the measurements. Note that the deflection shape can contain higher harmonic content. To define a damping ratio, a modal amplitude q is required, which is the scaling factor between the fundamental harmonics of mass-normalized and unscaled deflection shape, $\tilde{\boldsymbol{\psi}}_1 = q\tilde{\boldsymbol{\phi}}_1$. To compute the modal amplitude, linear mass-normalized mode shapes $\boldsymbol{\Phi}$ are required and obtained with a second measurement, a standard linear modal analysis (EMA) at low excitation level. With these, we can mass-normalize the nonlinear deflection shapes [14] and compute the modal amplitude with

$$q^2 = \tilde{\boldsymbol{\psi}}_1{}^{\mathrm{H}} \left(\boldsymbol{\Phi}^{\mathrm{T}}\right)^{+} (\boldsymbol{\Phi})^{+} \tilde{\boldsymbol{\psi}}_1. \tag{9}$$

Here, $()^{\mathrm{T}}$ is the transpose, $()^{\mathrm{H}}$ the Hermitian and $()^{+}$ the pseudo-inverse. To define a modal damping ratio, we assume that the dissipated power must be equal to the excitation power for a periodic motion [14]. Using only the fundamental harmonic component of the active power P_1 provided by the external force, the damping ratio is

$$\tilde{\zeta} = \frac{P_1}{\tilde{\omega}^3 q^2}. \tag{10}$$

2.2.3. Vibration Prediction

To predict steady-state vibrations, we set up the equation of a forced single-degree-of-freedom oscillator. In the frequency domain, we obtain the implicit equation

$$[-\Omega^2 + 2\mathrm{i}\Omega\tilde{\omega}\tilde{\zeta} + \tilde{\omega}^2] q \mathrm{e}^{\mathrm{i}\Delta\theta} = \mathrm{Re}\left\{\tilde{\boldsymbol{\phi}}_1{}^{\mathrm{H}} \boldsymbol{F}_{1,\mathrm{exc}}\right\}, \tag{11}$$

with amplitude-dependent $\tilde{\omega}(q)$, $\tilde{\boldsymbol{\phi}}_i(q)$ and $\tilde{\zeta}(q)$, the excitation frequency Ω and the phase of the modal coordinate $\Delta\theta$. In this work, we solve this equation numerically but note that it is also possible to write an explicit equation for $\Omega(q)$. $\boldsymbol{F}_{1,\mathrm{exc}}$ is the amplitude vector of the fundamental harmonic of the external forcing and assumed to be constant in the frequency range. In force-controlled experiments, often only the rms amplitude of the force is controlled and therefore constant for all frequencies. However, the influence of higher harmonics can vary in the amplitude range. It is possible to account for these variations in the vibration prediction by including fundamental harmonic content γ to the force amplitude [16].

Transient vibrations are predicted with slow-flow averaging [17]. The response of the system is described in terms of the modal amplitude, i.e. the magnitude $q(t)$ and the phase $\theta(t)$. From a known input force, described with the instantaneous magnitude $\boldsymbol{F}_{\mathrm{exc}}$ and frequency Ω, the response is given by the differential equations

$$\begin{bmatrix} \dot{q} \\ \dot{\theta} \end{bmatrix} = \frac{1}{2\Omega} \begin{bmatrix} -2\tilde{\zeta}\tilde{\omega}\Omega q - \tilde{\boldsymbol{\phi}}_1{}^{\mathrm{H}} \boldsymbol{F}_{\mathrm{exc}} \sin\theta \\ \tilde{\omega}^2 - \Omega^2 - \frac{1}{q}\tilde{\boldsymbol{\phi}}_1{}^{\mathrm{H}} \boldsymbol{F}_{\mathrm{exc}} \cos\theta \end{bmatrix}. \tag{12}$$

The main assumption for slow-flow averaging is slow variation of amplitude, phase lag and frequency compared to the oscillation. This makes slow-flow averaging an approximation even for linear models, which is an inherent limitation of the method.

3. Application to a Beam with Magnets

The first test specimen is a cantilever aluminum beam with the dimensions given in Fig. 2. Two ferrite magnets are attached near the free end, close to the node of the second bending mode. The magnets have a cylindrical shape and a residual induction of about 1.1 T. Opposite of these magnets, at a distance of $d_0 = 11\mathrm{mm}$, two magnets with

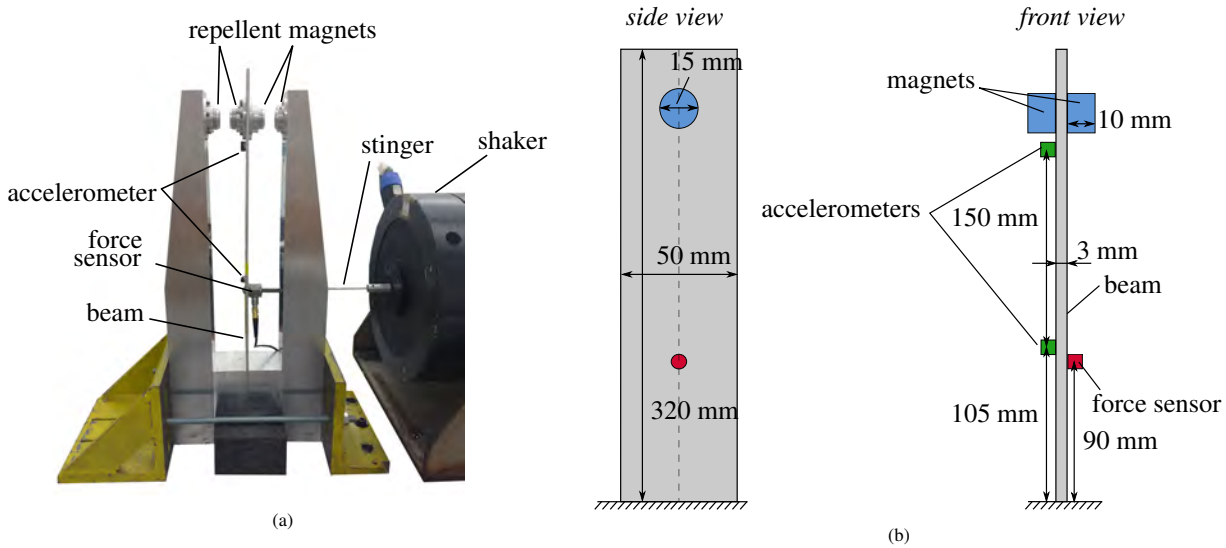

Figure 2: Picture (a) and scheme (b) of the aluminum beam with magnets and the experimental setup.

	Excitation	Purpose	Used platform / system
1	(stepped) sine	steady-state reference	dSPACE MicroLabBox
2	random noise (EMA)	nonlinear modal analysis	LMS Test.Lab / Siemens SCADAS Mobile
3	force appropriation (PLL)	nonlinear modal analysis	dSPACE MicroLabBox
4	multisine (identification)	PNLSS identification	LMS Test.Lab / Siemens SCADAS Mobile
5	multisine (characterization)	PNLSS identification	LMS Test.Lab / Siemens SCADAS Mobile
6	sine sweeps (uncontrolled)	transient reference	LMS Test.Lab / Siemens SCADAS Mobile

Table 1: Measurement campaign for the beam with magnets. For each measurement, the purpose and the measurement platform in use is stated. The measurements are listed in the order they were conducted.

same specifications are attached to a frame, causing a nonlinear magnetic repulsive force F acting between the magnet pairs [18],

$$F(x) = -\frac{K_0}{(d_0 - x)^4}. \tag{13}$$

The force depends on the deformation x of the beam at the height of the magnets in horizontal direction and a constant K_0 associated with the magnetic and geometrical properties. Due to the location of the magnets, the second mode is only slightly affected by the nonlinear force [19]. Therefore, the following experimental study focuses on the beam's first bending mode.

3.1. Experimental Setup

In all experiments, the excitation was applied with a Brüel & Kjær Vibration Exciter Type 4808 and a 100 mm long steel rod stinger, 2 mm in diameter. To measure the excitation force, a PCB 208C01 force sensor was screwed to the beam. Two uniaxial accelerometers (PCB 352A24) were glued to the beam, one close to the excitation location and one close to the magnets. All results in the following will be shown for the sensor close to the magnets.

The study's measurement campaign is composed by six different types of measurements: two for the nonlinear modal analysis, two for PNLSS identification and two types as reference measurements for subsequent vibration prediction. The different types are listed in Tab. 1, including the used measurement system and the order in which they were conducted. In the following sections, we describe the measurements in more detail.

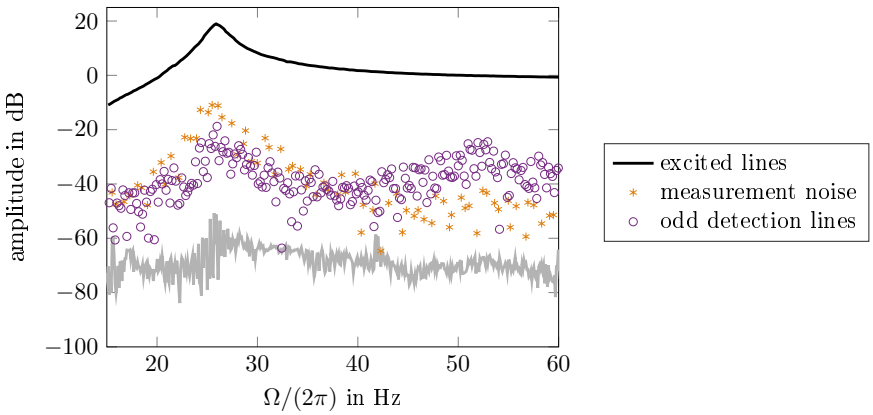

Figure 3: Characterization of the nonlinearity for the beam with magnets using detection lines. Both odd and even contributions are significant.

3.2. Identified Models

3.2.1. PNLSS Models

Prior to the identification, the system was excited at a high forcing level using a multisine signal with detection lines (cf. Section 2.1). Odd nonlinearities dominate the nonlinear response (see Fig. 3), but effects associated with even nonlinearities are also present at around twice the resonance frequency. Therefore, monomials of degree 2 and 3 are chosen as basis functions. Note that the polynomials can be interpreted as a Taylor series approximation of the nonlinear force (cf. Eq. (13)). Due to the truncation to order three, we expect the identified parameters to depend on the input, mainly the input level. To gather training data for the identification, the system was excited form 15 to 35 Hz with multisine signals at three different excitation levels, leading to excitation forces with rms amplitudes of 0.5 N, 2.6 N and 5.2 N, respectively. More details on the measurement setup such as number of measured realizations, sampling rate and recorded blocks are given in Appendix A.

Two states are sufficient to describe the system's dynamics around the isolated resonance. The measured excitation force was chosen as input and the acceleration at the two sensor locations are the outputs of the state-space model. Based on the gathered training data, different models can be identified: For every excitation level, one model is identified using eight realizations of the corresponding level. A fourth model, dubbed *mixed model*, is identified using training data concatenated of the various levels. In this case, the training data consists of three realizations of each excitation levels in ascending order. Note that no weighting is applied to account for different amplitude levels and severeness of errors.

To compare the quality of the different models, the error between the predicted response y_{sim} and a reference output y_{test} is computed. The reference is a measured realization not used in the identification procedure and the input of that realization is used to obtain the simulated response. As example, the (unnormalized) relative error of the mixed model is shown both in time and frequency domain in Fig. 4, where the reference data is a realization of the highest excitation level. The error shows a peak at about 24.6 Hz, just below the resonance frequency, but is otherwise 20 dB lower than the vibration level. The rms value of the error, normalized with the rms value of y_{test}, is then

$$e_{\text{rel}}^{\text{test}} = \frac{\sqrt{\frac{1}{N}\sum_{k=1}^{N}(y_{\text{test}}(k) - y_{\text{sim}}(k))^2}}{\sqrt{\frac{1}{N}\sum_{k=1}^{N} y_{\text{test}}(k)^2}}. \tag{14}$$

The relative errors for all models are listed in Tab. 2. All models have an error of less than 10 %, with the models of level 2.6 N rms and the mixed model having the lowest error. It is important to note that this error criteria evaluates how well each model performs on data of the *same* type, here multisine data.

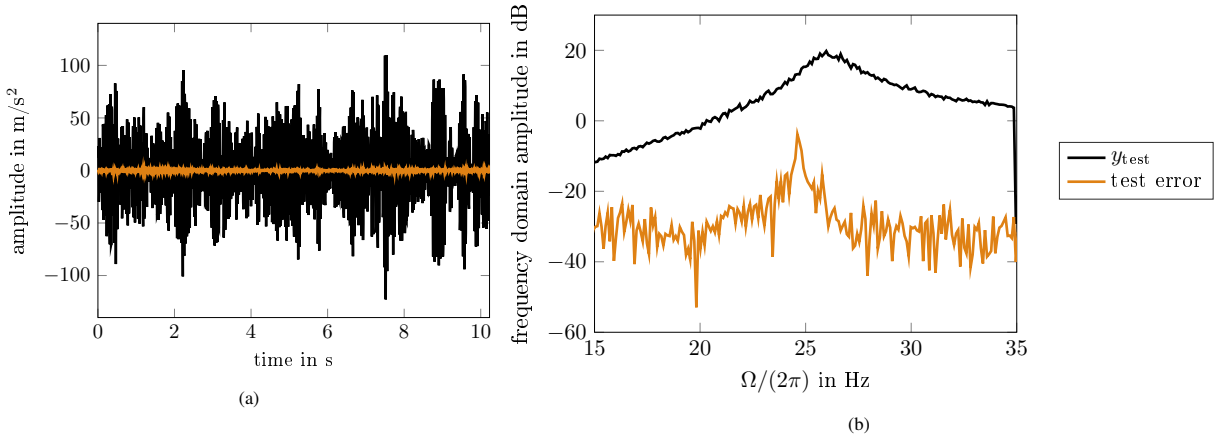

Figure 4: Relative errors in (a) time and (b) frequency domain of the mixed model compared with the reference output y_{test}. Note that the decibel is computed for amplitudes, i.e. $20\log_{10}(\cdot)$.

PNLSS with excitation multisine	0.5 N rms	2.6 N rms	5.2 N rms	mixed
$e_{\text{rel}}^{\text{test}}$	3.7 %	1.2 %	8.0 %	3.0 %

Table 2: Relative errors of the different PNLSS models according to Eq. (14). All models have errors less than 10 %.

3.2.2. Nonlinear Modal Model

As first step in the nonlinear modal analysis, an EMA was performed with pseudo-random excitation from 10 to 500 Hz. The first two bending modes were identified in this range (see Tab. 3). Both modes are lightly damped and well separated.

The backbone of the system was measured using the method described in Section 2.2.1. Details on the control parameters and other settings are given in Appendix A. We repeated the measurements four times and observed good repeatability with differences in the resonance frequency of different measurements of less than 0.1 %. The excited range lies between 0.026 N and 0.56 N force amplitude, corresponding to the amplitude of the fundamental harmonic. In this range, the measured vibration responses of the system are nearly mono-harmonic signals, but higher harmonics are significant in the excitation force for high amplitudes, with a fundamental harmonic content dropping to 0.93.

The identified modal properties depending on the amplitude are shown in Fig. 5. The resonance frequency increases by 3.7 %, revealing the stiffening effect of the magnetic force. Note that the resonance frequency is normalized with the linear natural frequency. The modal damping ratio increases by 6.7 % with increasing amplitude but seems to saturate for high amplitudes. However, the absolute damping values are small. Interestingly, the identified linear modal damping ratio of the first mode in Tab. 3 is equal to the average of the nonlinear damping. The amplitude dependence of the deflection shape is analyzed using the MAC value between the fundamental harmonic of the nonlinear deflection shape $\tilde{\boldsymbol{\phi}}_1$ and the linear mode shape $\boldsymbol{\phi}$ identified with EMA,

$$\text{MAC} = \frac{|\boldsymbol{\phi}^{\text{T}}\tilde{\boldsymbol{\phi}}_1|^2}{\boldsymbol{\phi}^{\text{T}}\boldsymbol{\phi}\,\tilde{\boldsymbol{\phi}}_1{}^{\text{H}}\tilde{\boldsymbol{\phi}}_1}. \tag{15}$$

	first bending mode	second bending mode
linear natural frequency	24.37 Hz	134.06 Hz
linear modal damping ratio	0.43 %	0.07 %

Table 3: Linear natural frequency and damping ratio for the first two bending modes, identified with EMA at low level.

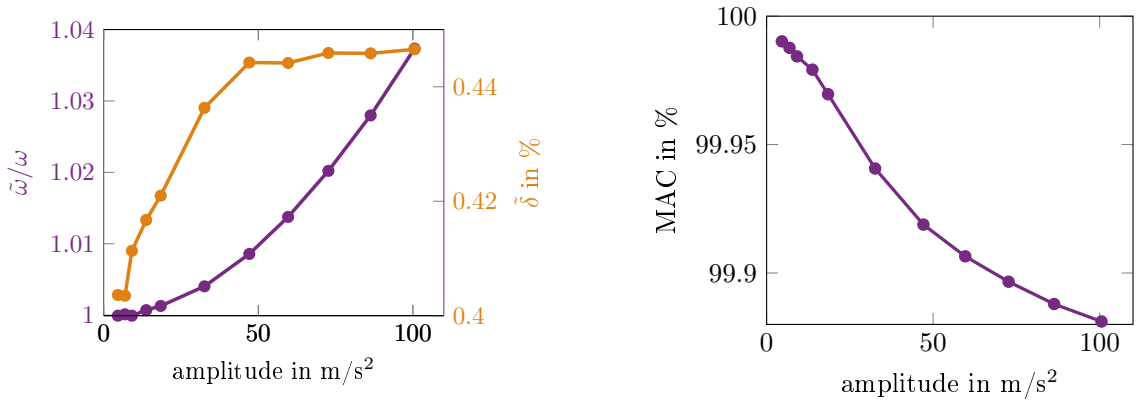

Figure 5: (a) Identified resonance frequency and modal damping ratio depending on the vibration amplitude. (b) MAC value between the linear deflection shape and the fundamental harmonic of the nonlinear deflection shape. Note that the shown amplitude corresponds to the fundamental harmonic and that the resonance frequency is normalized with the linear natural frequency of Tab. 3.

The MAC value decreases with amplitude but is close to one for all tested amplitudes (see Fig. 5), indicating that the deflection shape does not change significantly.

3.3. Vibration Prediction

We now investigate the capability of the identified models for vibration prediction of two different excitation types: steady-state harmonic excitation and sine sweeps through resonance.

3.3.1. Steady-state Oscillations

As reference, the system was excited with stepped sine signals. To this end, the phase lag between excitation force and drive-point acceleration was controlled using the PLL and varied around the resonance. Note that this is not the common stepped sine excitation where the excitation frequency is set. By controlling the phase lag, it is possible to stabilize and measure unstable branches of the frequency response [20]. The stable and unstable frequency response branch were measured separately for this specimen: The starting phase lag was about 95° with a subsequent increase or decrease for the stable and unstable branch, respectively. Four different excitation levels were tested, where the rms of the excitation force was controlled to the desired level. More details on the controller are given in Appendix A.

Two representative excitation levels are discussed in the following, namely 0.25 N and 0.55 N (see Fig. 6). The amplitude shown in the plot is again the magnitude of the fundamental harmonic. Both modal and PNLSS models capture well the general shape of the frequency response, including turning points. Therefore, both model types can generally be used for bifurcation analysis. However, the prediction accuracy of the different models regarding resonance frequency and maximal amplitude differ significantly. The nonlinear modal model predicts vibration that are very close to the measured response for both excitation levels with up to 1.2 % and 0.1 % error in amplitude and frequency, respectively. The *2.6 N rms* and the *mixed* PNLSS model yield the best predictions, which are equally good for the low excitation level (less than 2.5 % and 0.04 % error in amplitude and frequency, respectively). For the higher excitation level, the *2.6 N rms* model predicts amplitudes which are too high by 10.8 %, while the *mixed* model underestimates the amplitudes by 3.2 %. The *0.5 N rms* model also underestimates the amplitudes in both cases with errors up to 13.6 %. The PNLSS model identified at 5.2 N rms underestimates severely the maximum amplitude by up to 32.7 % and misses the resonance frequency by up to 1.6 %. Intuitively, one would expect this model to yield better predictions than a PNLSS model identified at lower excitation levels, especially for high excitation amplitude. However, this is not the case here. Note that the PNLSS models predicting steady-state responses best have the lowest relative errors $e_{\text{rel}}^{\text{test}}$. The model at 5.2 N rms has the highest error criteria and also underestimates the amplitude severely. Yet at this is point, it is still unclear if this correlation is a coincidence or if the error criteria $e_{\text{rel}}^{\text{test}}$ is indeed meaningful for prediction of harmonic signals.

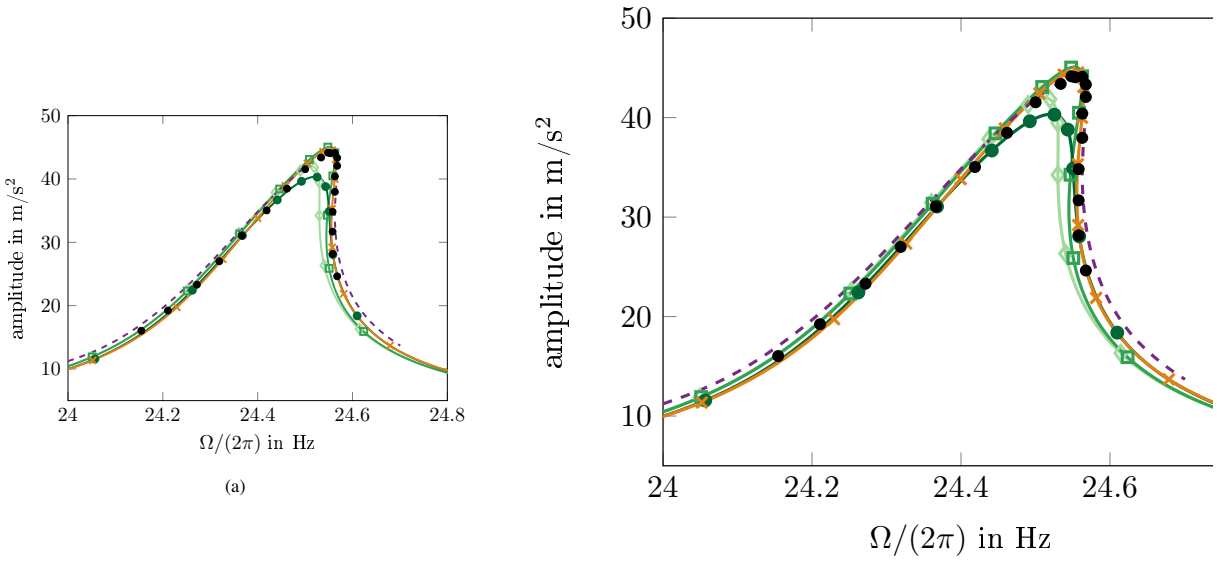

Figure 6: Vibration prediction of steady-state frequency responses for (a) 0.25 N and (b) 0.55 N excitation level. The prediction of both modal model and different PNLSS models are compared to a measured reference.

	model	amplitude error in m/s^2	amplitude error in [-] (relative)	frequency error in Hz	frequency error in [-] (relative)
0.25 N exc	PNLSS 0.5 N rms	-2.2	$-4.9 \cdot 10^{-2}$	$-3.6 \cdot 10^{-2}$	$-1.5 \cdot 10^{-3}$
	PNLSS 2.6 N rms	$9.4 \cdot 10^{-1}$	$2.1 \cdot 10^{-2}$	$4.2 \cdot 10^{-3}$	$1.7 \cdot 10^{-4}$
	PNLSS 5.2 N rms	-3.8	$-8.6 \cdot 10^{-2}$	$-2.8 \cdot 10^{-2}$	$-1.1 \cdot 10^{-3}$
	PNLSS mixed	$5.0 \cdot 10^{-1}$	$1.1 \cdot 10^{-2}$	$3.2 \cdot 10^{-3}$	$1.3 \cdot 10^{-4}$
	nonlinear modal model	$-2.5 \cdot 10^{-1}$	$-5.8 \cdot 10^{-3}$	$1.2 \cdot 10^{-3}$	$5.0 \cdot 10^{-5}$
0.55 N exc	PNLSS 0.5 N rms	-12.4	$-1.3 \cdot 10^{-1}$	$-2.4 \cdot 10^{-1}$	$-9.5 \cdot 10^{-3}$
	PNLSS 2.6 N rms	10.2	$1.1 \cdot 10^{-1}$	$1.5 \cdot 10^{-1}$	$6.0 \cdot 10^{-3}$
	PNLSS 5.2 N rms	-30.2	$-3.2 \cdot 10^{-1}$	$-4.1 \cdot 10^{-1}$	$-1.6 \cdot 10^{-2}$
	PNLSS mixed	-3.0	$-3.2 \cdot 10^{-2}$	$-8.4 \cdot 10^{-2}$	$-3.3 \cdot 10^{-3}$
	nonlinear modal model	1.1	$1.2 \cdot 10^{-2}$	$2.8 \cdot 10^{-2}$	$-1.1 \cdot 10^{-3}$

Table 4: Linear natural frequency and damping ratio for the first two bending modes, identified with EMA at low level.

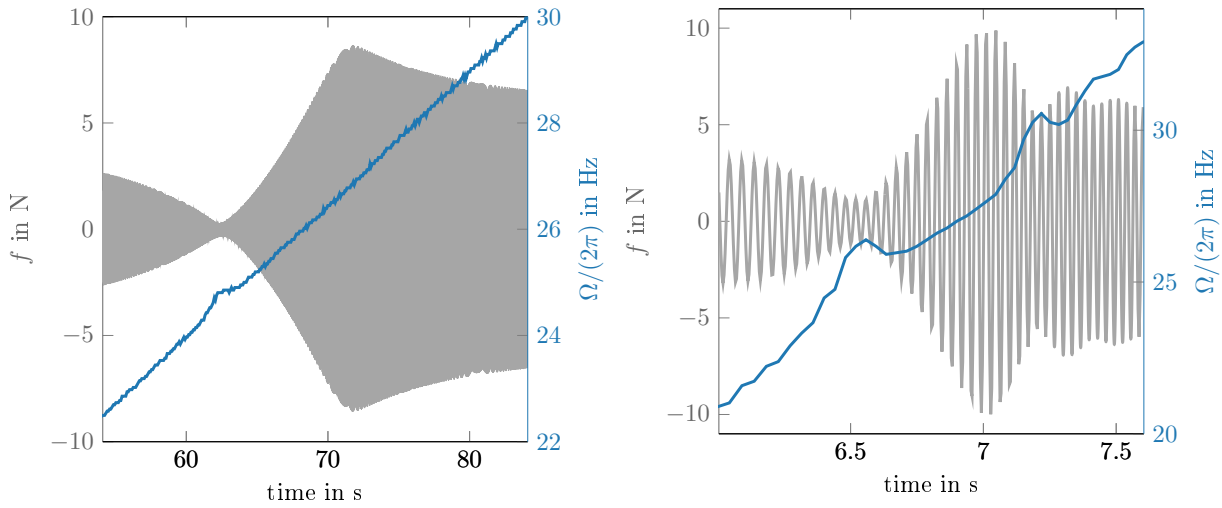

Figure 7: Measured excitation force and instantaneous excitation frequency for sweeps for two different sweep rates and 3.6 N excitation amplitude. Since the excitation force is not controlled, the actual force amplitude varies over time. Note that the variation in amplitude for the fast rate is not slow compared to the oscillation which violates assumption of slow-flow averaging. Note also that the instantaneous frequency does not increase linearly.

3.3.2. Transient Oscillations

As second test case, linear sine sweeps trough resonance from 10 to 40 Hz are predicted for two different sweep rates: Slow sweeps with 0.25 Hz/s and fast sweeps with 7.5 Hz/s. The sweep rates are associated with a 1 % frequency shift in the course of 23.75 and 0.79 periods, respectively, where the period is defined with the undamped linear natural frequency. The signals were sampled with 12 800 Hz. The sweeps are measured at three forcing levels for increasing frequencies only. Since the excitation force is not controlled, the actual force amplitude varies over time (see Fig. 7 for the medium forcing level). The excitation force amplitude for low frequencies (before resonance) for the three levels are approximately 0.4 N, 4.3 N and 6.5 N. Note that the variation in amplitude for the fast rate is no longer slow compared to the oscillation which violates the main assumption of slow-flow averaging.

To predict the vibration with PNLSS models, the measured force signal is used as input signal. For the nonlinear modal model, the slow-flow averaging algorithm requires time continuous functions for the instantaneous frequency and amplitude of the force signal (cf. Eq. (12)). To this end, the instantaneous frequency, shown in Fig. 7, is detected via the time difference between zero crossings. Note that even though the sweep rate was chosen to be linear, the instantaneous frequency extracted from the force signal does not show a linear increase, which is due to shaker-structure interactions. The maximum force value between two zero crossings is defined as instantaneous magnitude. Piecewise cubic Hermite polynomials were fitted to the extracted data to obtain time-continuous functions.

The predicted slow sweep responses for different excitation levels are shown in Fig. 8. Again, the predictions of PNLSS models of different training data levels differ significantly. For the lowest excitation level, the PNLSS models *0.5 N rms* and *2.6 N rms* predict the vibration well, whereas PNLSS model *5.2 N rms* and the *mixed* model show envelope modulation for frequencies lower than the resonance frequency, which we cannot explain. To asses the gain of using PNLSS models compared to a linear model, a single-degree-of-freedom modal model is set up based on the EMA results. The linear model predicts too high amplitudes (5 % of maximum amplitude). The nonlinear modal model predicts even higher amplitudes (9.5 % error), since the nonlinear damping is lower than linear damping for low energies (cf. Fig. 5 and Tab. 3). For the second excitation level, no model predicts the vibration with acceptable accuracy. The nonlinear modal model and the model *2.6 N rms* (not shown in Fig. 8b) are unstable, meaning the predicted amplitudes are close to or above MATLAB's value range. The *mixed* PNLSS model is not unstable but the predicted amplitudes are too high by factor 6. The PNLSS models *0.5 N rms*, *5.2 N rms*, and the linear model miss the resonance and show significant modulations in the envelope prior to the resonance. Also for the highest excitation level, no model is acceptable. Once more, the nonlinear modal model is unstable. All PNLSS models have envelope modulations and miss the frequency with maximal response. The linear model predicts the resonance at a

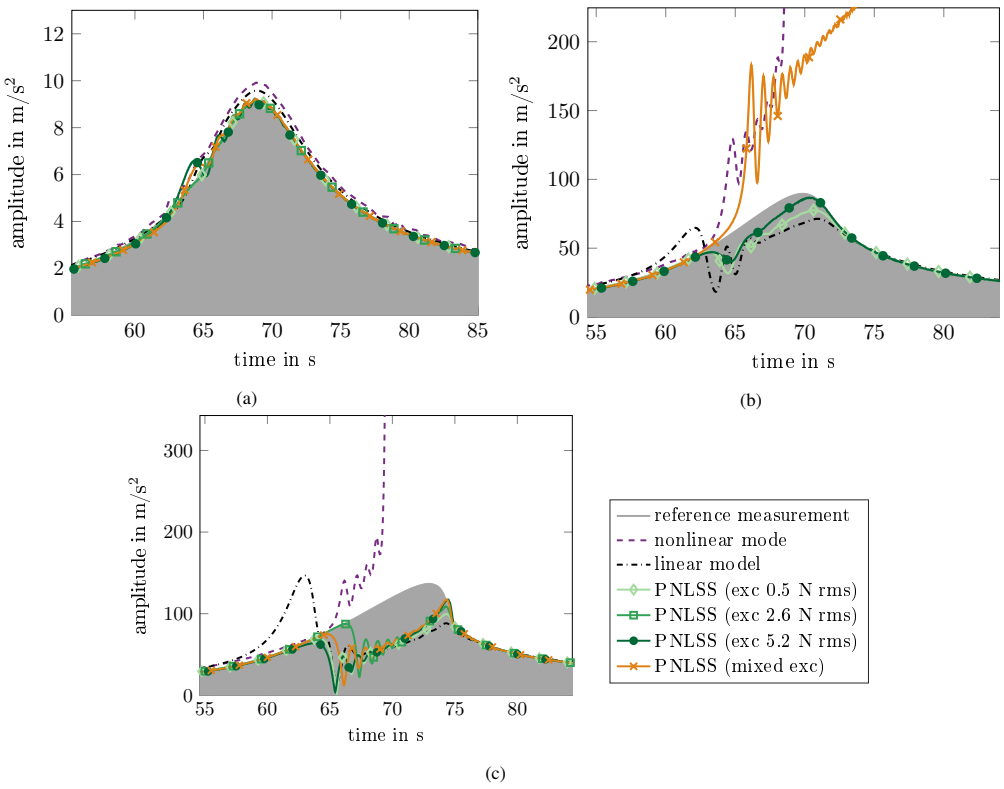

Figure 8: Prediction of slow sine sweeps for rms excitation levels (a) 0.4 N, (b) 4.3 N and (c) 6.5 N. The predictions of PNLSS models and nonlinear modal model are compared to the measured reference and to a linear model based on EMA data. Note that PNLSS model *2.6 N rms* is not shown in (b) since the model predicts unstable vibrations.

lower frequency since it cannot replicate the stiffening effect.

The results for the fast sweep rate are shown in Fig. 9 for the two higher forcing levels. For 4.3 N force amplitude, only the *mixed PNLSS* model and the model *2.6 N rms* predict with good precision (1.9 % and 0.5 % error in maximal amplitude, respectively). The other two PNLSS models underestimate the maximum amplitude by 13 % and 6 %. The linear model again misses the resonance and the nonlinear modal model overshoots and stays at too high amplitudes. For the highest forcing level, the *mixed* PNLSS model again predicts with good accuracy (0.5 % error). The other models miss the maximal amplitude and show modulations. The nonlinear modal predicts much too high amplitudes, the linear model misses the resonance.

To explain the unsuccessful prediction the nonlinear modal model, a numerical study was performed. In this section, only the major findings are stated; more details are given in Appendix B. One key effect is the force drop and subsequent overshoot of the excitation force seen in Fig. 7, which is associated with the transient nature of sweeps. If there is a small error in the model concerning the resonance frequency, the model sees a much higher excitation level at resonance frequency. This leads to a much higher response. Higher response amplitudes again lead to a higher resonance frequency due to the stiffening nonlinearity in the system. Therefore, the resonance condition is maintained, resulting in an unstable loop, which is generally known for stiffening systems and upward sweeps. Additionally, at high response levels, extrapolation of the modal properties can lead to wrong results.

3.3.3. Summary

As conclusion of the vibration prediction, one can summarize that the modal model performs much better for steady-state frequency responses but is not robust for transient sweeps. Generally, the PNLSS models that perform good in steady-state frequency response predictions perform also good on sweep predictions. However, no model is consistently good. Neither the mixed nor the 2.6 N rms PNLSS model performs well on all sweeps. They can even

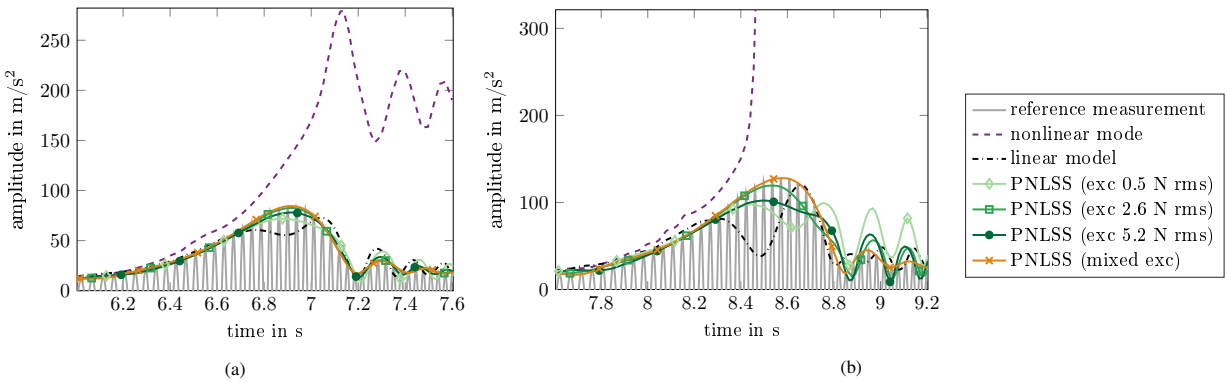

Figure 9: Prediction of fast sine sweeps for the rms excitation levels (a) 4.3 N and (b) 6.5 N. The predictions of PNLSS models and nonlinear modal model are compared to the measured reference and to a linear model based on EMA data.

	model	exc 0.4 N	exc 2.6 N	exc 5.2 N
slow sweep	PNLSS 0.5 N rms	$8.8 \cdot 10^{-3}$	$1.7 \cdot 10^{-1}$	$3.9 \cdot 10^{-1}$
	PNLSS 2.6 N rms	$9.4 \cdot 10^{-3}$	unstable	$3.2 \cdot 10^{-1}$
	PNLSS 5.2 N rms	$4.0 \cdot 10^{-2}$	$1.1 \cdot 10^{-1}$	$3.8 \cdot 10^{-1}$
	PNLSS mixed	$2.5 \cdot 10^{-2}$	unstable	$3.5 \cdot 10^{-1}$
	nonlinear modal model	$7.8 \cdot 10^{-2}$	unstable	unstable
	linear model	$4.5 \cdot 10^{-2}$	$2.4 \cdot 10^{-1}$	$4.7 \cdot 10^{-1}$
fast sweep	PNLSS 0.5 N rms		$1.3 \cdot 10^{-1}$	$3.4 \cdot 10^{-1}$
	PNLSS 2.6 N rms		$1.2 \cdot 10^{-2}$	$1.2 \cdot 10^{-1}$
	PNLSS 5.2 N rms		$5.9 \cdot 10^{-2}$	$1.9 \cdot 10^{-1}$
	PNLSS mixed		$1.6 \cdot 10^{-2}$	$1.6 \cdot 10^{-2}$
	nonlinear modal model		2.8	unstable
	linear model		$2.1 \cdot 10^{-1}$	$3.6 \cdot 10^{-1}$

Table 5: Linear natural frequency and damping ratio for the first two bending modes, identified with EMA at low level.

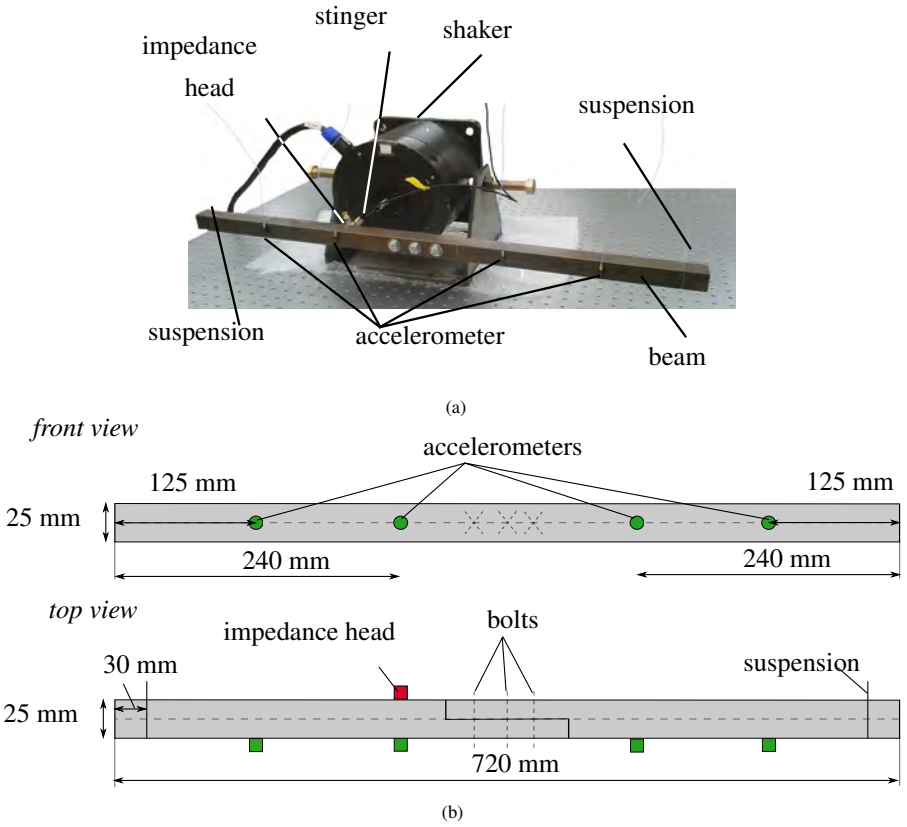

Figure 10: Picture (a) and scheme (b) of the BRB and the experimental setup.

become unstable. It is therefore still unclear which excitation level should be chosen in the training data since no clear trend is visible. The test error $e_{\text{rel}}^{\text{test}}$ seems to give a hint for the prediction capability of steady-state responses but not for transient sweeps. The mixed model seems to be the model with the widest validation regime but this observation is not generally valid. Note that PNLSS models seem to predict faster sweeps better than slow sweeps, since fast sweeps are more similar to the training data than slow, almost steady-state sweeps.

4. Application to the BRB

4.1. Experimental Setup

The second test specimen is the BRB which is assembled from two beams, jointed by three bolts with washers [1]. The degree of nonlinearity in the jointed interface depends on the bolt torque [21]. In this work, a relatively small bolt torque of 5 Nm was chosen to enhance nonlinear behavior. Unlike for the beam with magnets, we cannot easily model the nonlinear force acting in the joint. Only the first bending mode is investigated in this study. Note that the beam was kept assembled between the measurements.

Again, the excitation was applied using shaker-stinger excitation in the lateral direction with a 2 diameter steel rod of 65 mm length and the Brüel & Kjær Vibration Exciter 4808. Four PCB 352A24 uniaxial accelerometers were glued and one PCB 288D01 impedance head was screwed to the beam at the locations indicated in Fig. 10. In the following, the sensor on the right side of the joint is chosen as representative channel. The beam was suspended with nylon strings and bungee chords.

For this test specimen, the measurement campaign is composed of seven different types of measurement (see Tab. 6): two for the nonlinear modal analysis, two for PNLSS identification and three types as reference measurements for the subsequent vibration prediction.

	Excitation	Purpose	Used platform
1a	(stepped) sine	steady-state reference	dSPACE MicroLabBox
1b	slow sine sweeps (controlled)	steady-state reference	LMS Test.Lab / Siemens SCADAS Mobile
2	random noise (EMA)	nonlinear modal analysis	LMS Test.Lab / Siemens SCADAS Mobile
3	force appropriation (PLL)	nonlinear modal analysis	dSPACE MicroLabBox
4	multisine (identification)	PNLSS identification	LMS Test.Lab / Siemens SCADAS Mobile
5	multisine (characterization)	PNLSS identification	LMS Test.Lab / Siemens SCADAS Mobile
6	fast sine sweeps (uncontrolled)	transient reference	LMS Test.Lab / Siemens SCADAS Mobile

Table 6: Measurement campaign for the BRB. For each measurement, the purpose and the measurement platform in use is stated. The measurements are listed in the order they were conducted.

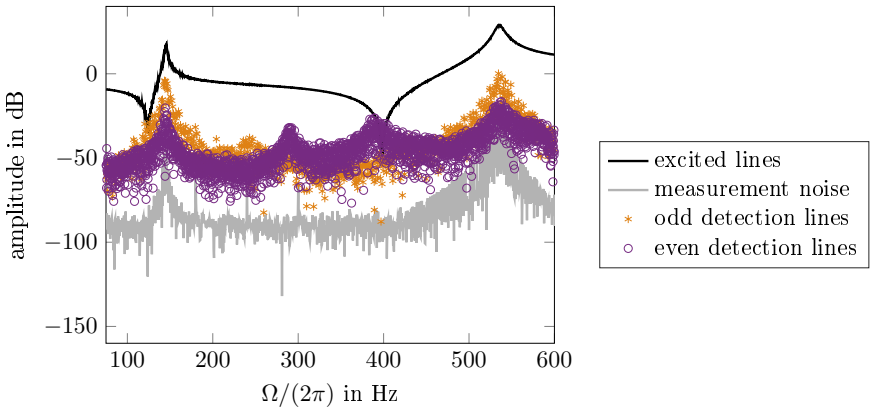

Figure 11: Characterization of the nonlinearity for the BRB using detection lines. Both odd and even contributions are significant.

4.2. Identified Models

4.2.1. PNLSS Models

Prior to the identification, we characterized the nonlinearity using detection lines. Odd nonlinearities dominat the response at resonance but influence of even nonlinearities is present at twice the fundamental frequency (see Fig. 11). Therefore, polynomials of degree 2 and 3 are included in the model.

Multisine excitation with the specification given in Appendix A was applied to the beam around the first resonance from 75 to 225 Hz. We tested at four excitation levels, having approximately rms amplitudes of 10 N, 20 N, 30 N, and 50 N. The models were identified based on eight realizations of the training data. The identified PNLSS models have one input and four outputs corresponding to the excitation force and the measured accelerations. Note that the acceleration recorded by the impedance head at the drive point was considered, discarding the accelerometer data. Since an antiresonance appears just before the first resonance, four states are necessary to replicate the dynamics. Again, one PNLSS model was identified for each excitation level as well as one mixed model with concatenating data in ascending order without weighting. Here, three realization of each level were included. The mixed model is tested on a realization of the highest excitation level, (see Fig. 12). The error is about 25 dB below the response at resonance. At the antiresonance, the error is of similar level than the response.

In the following, only the mixed model and the models *10 N*, *30 N* and *50 N* are shown as representative results. To compare the identified models, the relative error measure $e_{\mathrm{rel}}^{\mathrm{test}}$ of Eq. (14) is applied, stated in Tab. 7. All models are below 10 % relative error with PNLSS model 10 N rms having the lowest error.

4.2.2. Nonlinear Modal Model

A linear EMA was performed, exciting the frequency range from 100 to 2000 Hz with a pseudo-random multisine signal. Four well-separated modes were identified in this range (see Tab. 8).

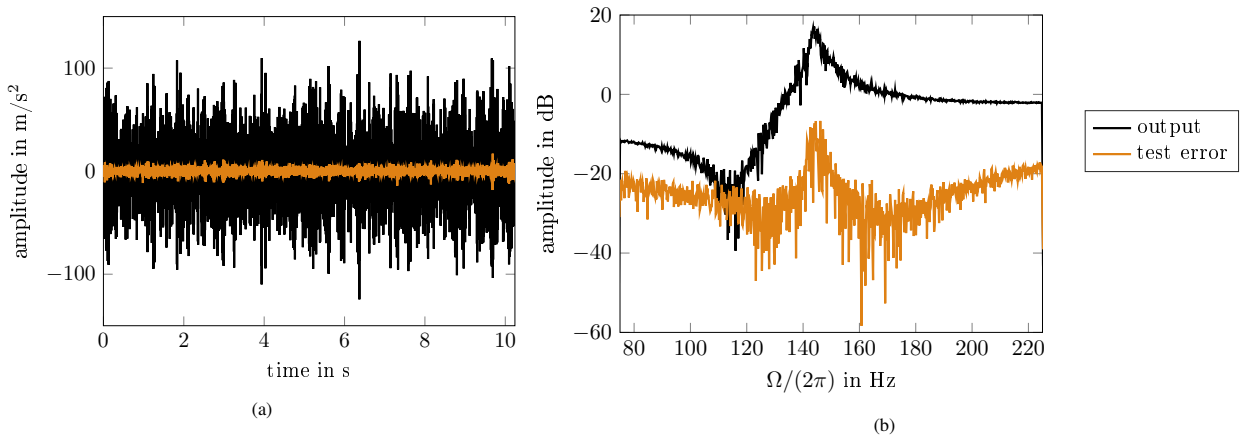

Figure 12: Relative errors in (a) time and (b) frequency domain of the mixed model compared with the reference output. Note that the decibel is computed for amplitudes, i.e. $20\log_{10}(\cdot)$.

PNLSS with excitation multisine	10 N rms	30 N rms	50 N rms	mixed
$e_{\mathrm{rel}}^{\mathrm{test}}$	2.7 %	4.8 %	7.3 %	8.2 %

Table 7: Relative errors of the different PNLSS models according to Eq. (14). All models have errors less than 10 %.

For the nonlinear modal analysis of the first mode (first bending mode), we measured five backbones. Good repeatability was observed for the measured frequencies (below 0.1 %) but a variation of about 2 % for the amplitudes was present. The modal model is identified for one of the measured backbones evaluated at eleven excitation levels from 0.1 N to 16.6 N amplitude. Details on the measurements are given in Appendix A. As can be seen in Fig. 13, the resonance frequency decreases by 2.2 % over the amplitude range while the damping ratio increases significantly. Note that the resonance frequency in Fig. 13 is normalized with the linear natural frequency. The distortion factor of the excitation force is low (0.74) for the backbone point with the lowest amplitudes due to a bad signal to noise ratio. For all other amplitudes, the distortion factor is above 0.96. The deflection shape does not change significantly with increasing amplitude because the MAC value (cf. Eq. (15)) is close to one in the tested amplitude regime (see Fig. 13).

4.3. Vibration Prediction

4.3.1. Steady-state Oscillations

As reference measurements, we preformed sine measurements with phase control and controlled excitation force. We tested five levels, starting at the highest excitation level. Additionally, we applied force-level-controlled sine sweeps were performed from 142 to 151 Hz at the same force levels. Here, the sweep rate was 0.03 Hz/s, which correlates to a 1 % change in frequency in about 7403 periods. These sweeps validate the measured phase-controlled steady-state frequency responses. The sweeps were sampled with 3200 Hz.

The results are shown for three representative levels, namely for the levels 2 N, 5 N, and 15 N. The modal model predicts too small amplitudes for the excitation levels 2 N and 5 N (see Fig. 14). For the highest excitation level, the amplitudes and the resonance frequency differ only slightly from the reference measurements (2.7 % amplitude error).

	mode 1	mode 2	mode 3	mode 4
linear natural frequency	149.0 Hz	564.3 Hz	1138.3 Hz	1496.5 Hz
linear modal damping ratio	0.14 %	0.05 %	0.08 %	0.11 %

Table 8: Linear natural frequency and damping ratio for the first four modes, identified with EMA at low level.

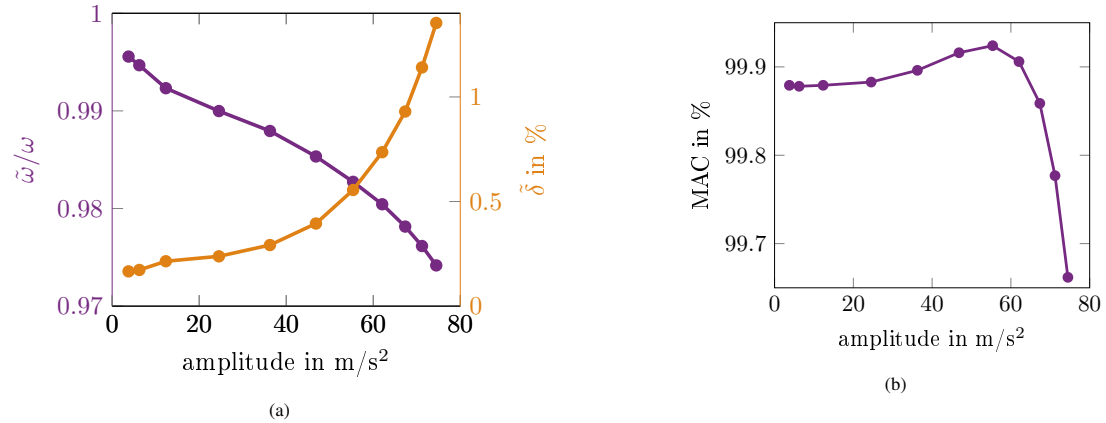

Figure 13: (a) Identified resonance frequency and modal damping ratio depending on the vibration amplitude. (b) MAC value between the linear deflection shape and the fundamental harmonic of the nonlinear deflection shape. Note that the amplitude corresponds to the fundamental harmonic.

All PNLSS models significantly underestimate the maximum amplitude for 2 N excitation level with errors between 19.4 % and 29.1 %, where the predicted resonance frequency differs between models. For 5 N and 15 N excitation level, all PNLSS models but one underestimate the maximum amplitude by 9.1 % to 27.3 %. Only PNLSS model *10 N rms* predicts the amplitude for 5 N excitation with good accuracy (0.5 % error) and only slightly misses the resonance frequency. The vibration prediction is in fact better than the one of the modal model. For 15 N excitation, in contrast, the predicted response amplitudes of PNLSS model *10 N rms* are much too high (factor 4).

Some deviation between prediction and reference can be attributed to the inherent variability of systems with joints. Potentially, the interface at the joint changed due to contact interactions between the reference measurements and the backbone or multisine measurements, performed after the stepped sine. If one, for example, compares measured points of the backbone to points of the sine measurements at the same excitation force and the same phase lag, the response amplitudes in the frequency response are larger than in the backbone measurement, indicating a slight change in the system dynamics.

The high variability of predictions of PNLSS models could also stem from the input dependence of the model parameters. It is clear that nonsmooth nonlinearities cause by contact interactions at the interface are not correctly modeled by polynomials. By choosing only few polynomial terms, we approximate to a large degree, introducing inherent errors to the model. Further research is necessary to investigate whether more polynomial terms would significantly improve the models and their prediction quality. It is interesting that the *mixed* model seems to perform better in the prediction than models *30 N rms* and *50 N rms* even though the *mixed* model has the largest testing errors $e_{\text{rel}}^{\text{test}}$, (see Tab. 7). In contrast, the model with the smallest error $e_{\text{rel}}^{\text{test}}$, model *10 N rms*, fails to predict the highest amplitudes and it seems that the model's valid regime is exceeded. The accurate prediction of vibrations with 5 N excitation might be a coincidence. Since we cannot reliably distinguish between good models or lucky coincidences, we have to be careful with conclusions based on these results. However, we can note that the prediction quality does not clearly correlate with the testing error $e_{\text{rel}}^{\text{test}}$ for this test specimen.

4.3.2. Transient Oscillations

For the BRB, only fast sine sweeps were measured with excitation at six different levels. The sweep rate was 15 Hz/s from 130 to 190 Hz, corresponding to a 1 % frequency shift in 14.81 periods. The sweeps are uncontrolled which lead to variation of the excitation force, especially to oscillations after resonance (see Fig. 15). The sampling rate was 12800 Hz. To obtain time-continuous instantaneous magnitude and frequency of the excitation force, we followed the procedure described in Section 3.3.2.

The results are shown in Fig. 16 for two representative levels with 8.1 N and 19.1 N force amplitude at low frequencies. The *mixed* PNLSS model is the best of all PNLSS models. It accurately predicts the low level sweep and has a good agreement with the high level sweep with 2.2% amplitude error. PNLSS model *30 N rms* predicts with satisfying accuracy (up to 4 % error). The amplitudes predicted with PNLSS model *10 N rms* are too high by 2.9 %

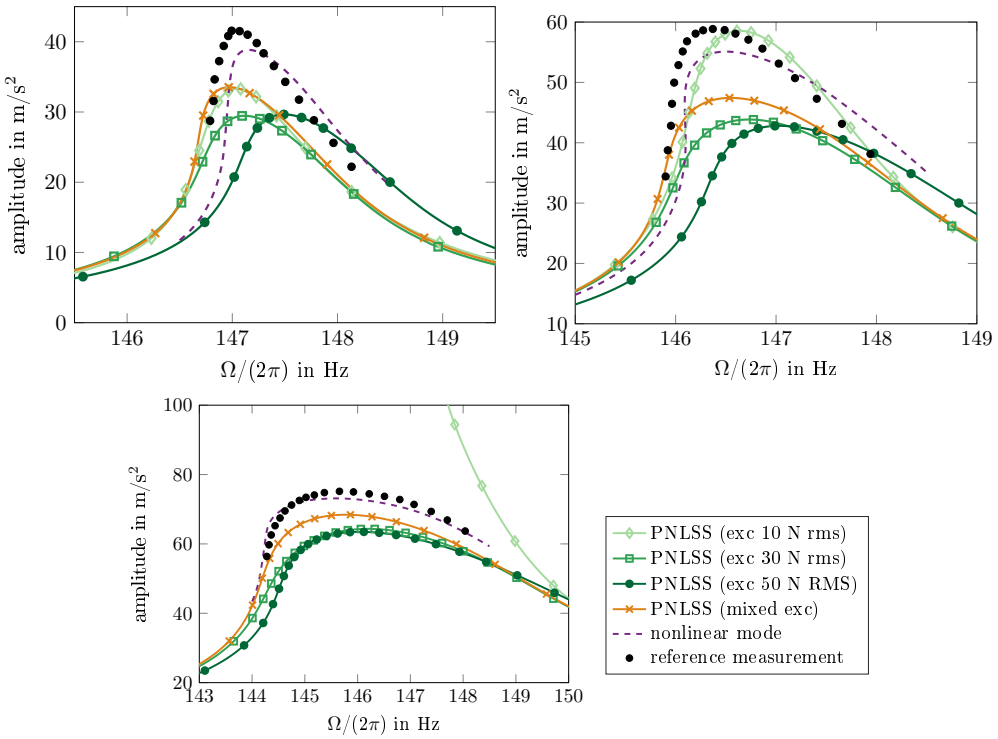

Figure 14: Vibration prediction of steady-state frequency responses for (a) 2 N, (b) 5 N and (c) 15 N excitation level. The prediction of both modal model and different PNLSS models are compared to a measured reference.

	model	amplitude error in m/s^2	amplitude error in [-] (relative)	frequency error in Hz	frequency error in [-] (relative)
2 N exc	PNLSS 10 N rms	-8.2	$-2.0 \cdot 10^{-1}$	$5.1 \cdot 10^{-2}$	$3.5 \cdot 10^{-4}$
	PNLSS 30 N rms	-12.1	$-2.9 \cdot 10^{-1}$	$1.2 \cdot 10^{-1}$	$8.3 \cdot 10^{-4}$
	PNLSS 50 N rms	-11.9	$-2.9 \cdot 10^{-1}$	$5.0 \cdot 10^{-1}$	$3.4 \cdot 10^{-3}$
	PNLSS mixed	-8.0	$-1.9 \cdot 10^{-1}$	$-1.9 \cdot 10^{-2}$	$-1.3 \cdot 10^{-4}$
	nonlinear modal model	-2.7	$-6.6 \cdot 10^{-2}$	$1.7 \cdot 10^{-1}$	$1.1 \cdot 10^{-3}$
5 N exc	PNLSS 10 N rms	$-2.9 \cdot 10^{-1}$	$-5.0 \cdot 10^{-3}$	$2.7 \cdot 10^{-1}$	$1.8 \cdot 10^{-3}$
	PNLSS 30 N rms	-15.0	$2.6 \cdot 10^{-1}$	$3.6 \cdot 10^{-1}$	$2.5 \cdot 10^{-3}$
	PNLSS 50 N rms	16.0	$-2.7 \cdot 10^{-1}$	$6.6 \cdot 10^{-1}$	$4.5 \cdot 10^{-3}$
	PNLSS mixed	-11.4	$-1.9 \cdot 10^{-1}$	$1.8 \cdot 10^{-1}$	$1.2 \cdot 10^{-3}$
	nonlinear modal model	-3.7	$-6.4 \cdot 10^{-2}$	$1.3 \cdot 10^{-1}$	$8.8 \cdot 10^{-4}$
15 N exc	PNLSS 10 N rms	294.7	3.9	-5.7	$-3.9 \cdot 10^{-2}$
	PNLSS 30 N rms	-10.8	$-1.4 \cdot 10^{-1}$	$5.4 \cdot 10^{-1}$	$3.7 \cdot 10^{-3}$
	PNLSS 50 N rms	-11.7	$-1.6 \cdot 10^{-1}$	$3.9 \cdot 10^{-1}$	$2.7 \cdot 10^{-3}$
	PNLSS mixed	-6.7	$-9.0 \cdot 10^{-2}$	$1.2 \cdot 10^{-1}$	$8.4 \cdot 10^{-4}$
	nonlinear modal model	-2.0	$-2.7 \cdot 10^{-2}$	$-5.9 \cdot 10^{-2}$	$-4.0 \cdot 10^{-4}$

Table 9: Linear natural frequency and damping ratio for the first two bending modes, identified with EMA at low level.

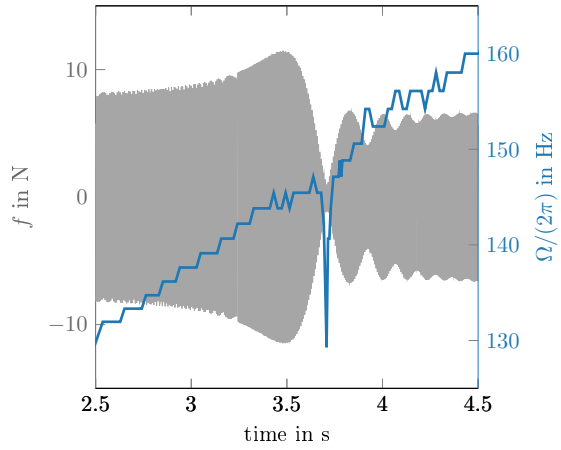

Figure 15: Measured excitation force and instantaneous excitation frequency in sweeps. Since the excitation force is not controlled, the actual force amplitude varies over the frequency range. Note that the instantaneous frequency does not increase linearly.

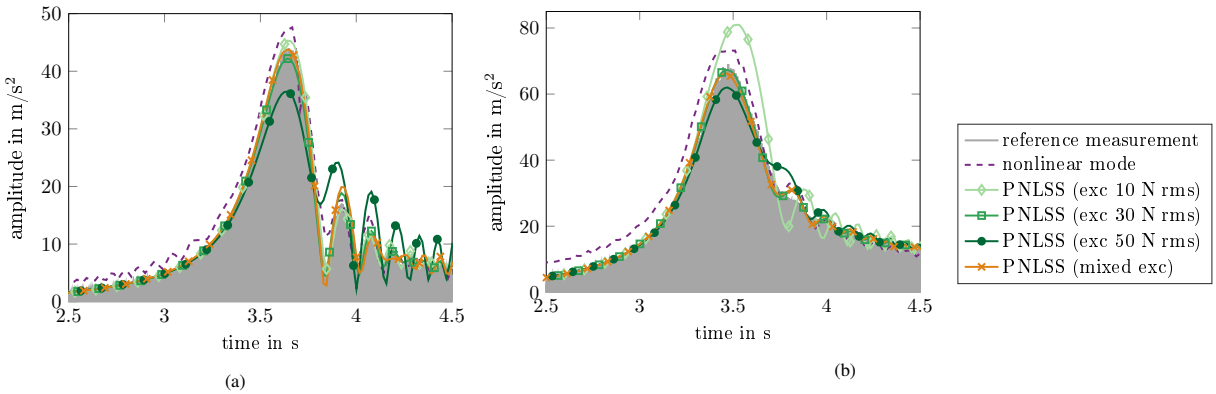

Figure 16: Prediction of sine sweeps for two different excitation levels. The predictions of PNLSS models and nonlinear modal model are compared to the measured reference.

and 19.5 %, respectively. PNLSS model *50 N rms* both predicts too low amplitudes (17.2 % and 8.8 % error) and too pronounced amplitude modulations after the resonance. The relative error $e_{\text{rel}}^{\text{test}}$ does not correlate with the prediction. On the one side, the *mixed* model performs best though it has the highest value of $e_{\text{rel}}^{\text{test}}$. On the other side, the sweep predictions of model *10 N rms* with the lowest error are not satisfying. The accuracy of the nonlinear modal model is moderate (about 8 % amplitude error) but does not suffer from the limitations seen in the beam specimen.

5. Conclusions

In this paper, two different nonlinear system identification methods, PNLSS identification and a nonlinear modal method, with fundamentally different excitation signals were applied and compared with respect to their predictive capabilities. We only investigated vibrations near an isolated resonance. Regarding the experimental effort for the two methods we observed that the modal approach requires an controller which needs to be tuned prior to the measurements. The measurement duration depends on this tuning. The measurements for PNLSS identification can be readily set up with commercial testing packages that offer multisine excitation.

On the one side, the modal model is identified based on harmonic vibrations. The model is only valid around an isolated resonance which is a clear model limitation. One the other side, we identified PNLSS models using random broadband data. Since the nonlinear basis functions generally only approximate the nonlinearity, the identified

model	exc 5.6 N	exc 7.9 N
PNLSS 10 N rms	$3.3 \cdot 10^{-2}$	$1.9 \cdot 10^{-1}$
PNLSS 30 N rms	$6.3 \cdot 10^{-2}$	$4.0 \cdot 10^{-2}$
PNLSS 50 N rms	$2.4 \cdot 10^{-1}$	$9.7 \cdot 10^{-2}$
PNLSS mixed	$6.7 \cdot 10^{-2}$	$4.8 \cdot 10^{-2}$
nonlinear modal model	$1.5 \cdot 10^{-1}$	$1.7 \cdot 10^{-1}$

Table 10: Linear natural frequency and damping ratio for the first two bending modes, identified with EMA at low level.

test specimen	purpose	sampling frequency	# blocks	realizations	excited range
beam with magnets	identification	800 Hz	20	10	15 - 35 Hz
	characterization	800 Hz	20	-	15 - 220 Hz
BRB	identification	6400 Hz	25	10	75 - 225 Hz
	characterization	6400 Hz	25	-	75 - 600 Hz

Table A.1: Measurement settings for multisine signals. Multisine signal for identification are without detection lines; multisine signals for characterization include detection lines.

parameters depend on the training data. Therefore, the level of excitation must be chosen carefully. However, we found no clear indication how the level of *random* training data must be chosen to predict *harmonic* vibrations

The modal model performs well for predictions of steady-state harmonic responses both for stiffening and damping nonlinearities. The transient vibrations have only moderate accuracy and seem to be sensitive to model errors. Especially in cases where the system is stiffening and uncontrolled upward sweeps are predicted, the modal model fails to predict sweeps.

The vibration prediction of PNLSS models differ depending on the level of the training data. Using training data of concatenated vibration levels seems to improve the model's validity but still the model might fail at certain harmonic levels. Transients sweeps are generally predicted with higher accuracy, especially for fast sweep rates. However, no PNLSS model performed consistently well. We did not find a general correlation between an error criteria based on random broadband signals, $e_{\mathrm{rel}}^{\mathrm{test}}$, and the prediction quality.

The drawn conclusions are only based on two different test specimens. We do not have enough data to support final conclusions regarding the predictive capabilities of both methods. It seems that the strength of each method lies in predicting vibrations similar to the training data (periodic steady-state vs. broadband around resonance). However, more work is needed to verify this observation.

Acknowledgment

This work was funded by the Deutsche Forchungsgemeinschaft (DFG, German Research Foundation) - Project 402813361.

Appendix A. Parameters of Measurement setup

The settings of all multisine signals are given in Tab. A.1 for both test specimens. Note that multisine signals used for characterization include detection lines.

For the nonlinear modal analysis, the PLL controller sketched in Fig. A.1a was used. For the reference measurement with stepped sines, the PLL was extended with a control loop for the force amplitude (see Fig. A.1b). The parameters for the controller are given in Tab. A.2. Details on the measurements with PLL are given in Tab. A.3, including the sampling frequency and the tested amplitude levels. For each tested amplitude level in the backbone

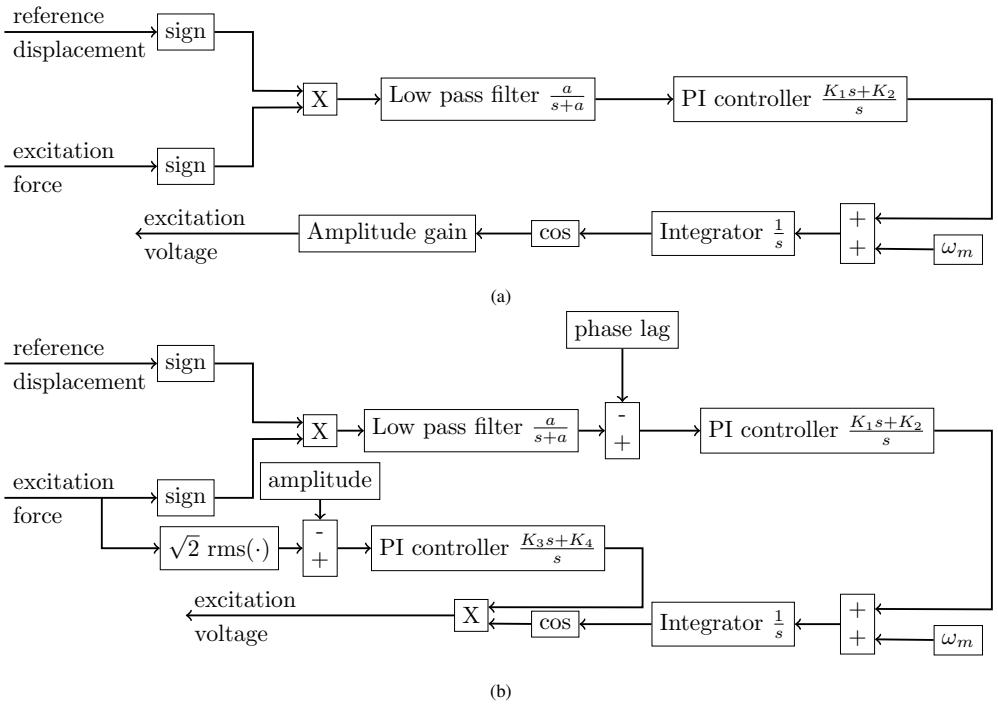

Figure A.1: Scheme of PLL controller used for (a) nonlinear modal analysis and (b) stepped-sine measurements. The PLL in (b) is extended with a controller for the force amplitude. The parameters are given in Tab. A.2.

test specimen	measurement	a	K_1	K_2	K_3	K_4	ω_m
beam with magnets	stepped sine	2π	2	2π	1.5	1	48π rad/s
	backbone	2π	2	2π	-	-	48π rad/s
BRB	stepped sine	2π	1	10π	5	1	300π rad/s
	backbone	2π	1	10π	-	-	290π rad/s

Table A.2: Control parameters for measurements with PLL.

measurements, the excitation is held for certain time (*waiting time*) to ensure that steady state is reached. Then, a certain number of periods are recorded for the subsequent analysis. The same procedure is applied for the stepped-sine measurements, where the phase lag is kept constant.

Appendix B. Numerical Investigation of Transient Sweeps

In Section 3.3.2, we observed that the nonlinear modal model is not capable of predicting sweeps, but instead often predicts unstable vibrations. To explain this behavior, we study a numerical single-degree-of-freedom oscillator with cubic spring. The parameters are chosen to represent the measured backbone curve and frequency responses around the first resonance of the beam with magnets. Additional to the nominal model, two models with erroneous modal characteristics are studied: One with random errors of the resonance frequency and one with a constant positive offset of 0.5 % of the resonance frequency (see Fig. B.1). In absolute values, this correlates to a 0.1 Hz shift for the beam with magnets. All three models are now used to predict vibrations under sine sweep excitation using the slow-flow averaging procedure described in Section 2.2.3. To this end, the instantaneous frequency and magnitude of the measured excitation forces for both fast and slow sweep rates are used as input. For reference, the nominal model's sweep response to the same excitation forces is simulated using MATLAB/Simulink. For the slow sweep rate, the

test specimen	measurement	sampling frequency	phase lag	amplitude levels in N	waiting time	recorded periods
beam with magnets	stepped sine	5000 Hz	95° ... 153° 95° ... 26°	$\{0.1, 0.25, 0.4, 0.55\}$	53 s	50
	backbone	5000 Hz	90°	0.26 ... 0.56	48 s	50
BRB	stepped sine	5000 Hz	160° ... 27°	$\{1, 2, 5, 10, 15\}$	25 s	200
	backbone	5000 Hz	90°	0.1 ... 16.6	30 s	200

Table A.3: Measurement settings for PLL measurements with both specimens. The waiting time refers to the time span each step was held with constant excitation to reach steady state. Then, the number of recorded periods are recorded for the subsequent analysis. Note that the given force amplitudes refer to amplitudes of purely sinusoidal signals.

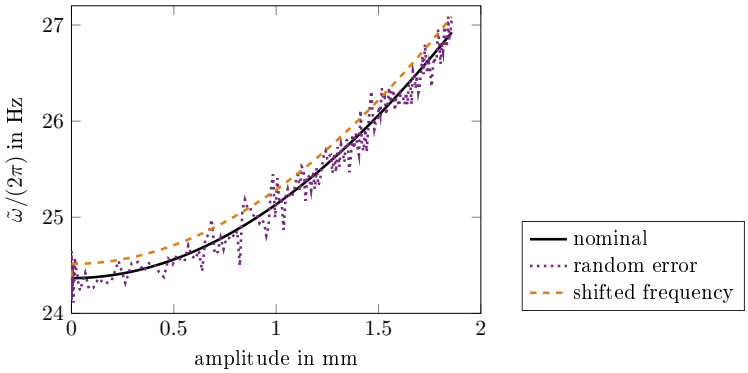

Figure B.1: Amplitude dependent resonance frequency of a one-mass oscillator resembling the beam with magnets. Besides the nominal model, a model with random errors and a model with a constant error are used.

nominal model's sweep prediction matches the reference solution very well (see Fig. B.2a). The prediction of the model with random errors does not match the reference but the amplitudes stay bounded. For the fast sweep (see Fig. B.2b), the predicted response of both nominal model and model with random errors deviate from the reference but the general response is captured. The deviation can be attributed to the fast change in amplitude, violating the assumption of slow-flow averaging. However, this violation does not cause unstable responses for this system. Only the model with the shifted resonance frequency predicts unstable vibration responses for both slow and fast sweeps. If the resonance frequency are predicted just slightly too high, the system exhibits a significant higher force at resonance due to the increase in forcing amplitude after resonance. This then leads to higher amplitudes of the system which then increases the resonance frequency due to the stiffening nonlinearity. The resonance condition is therefore maintained. To confirm this explanation, we predict sweeps with a constant forcing level. As expected, all predicted responses stay bounded (see Fig. B.3). One therefore has to be cautious when predicting sweeps with slow-flow-averaging for experimentally identified models with uncontrolled force drop. This applies especially for systems with low damping, stiffening nonlinearities and forward sweeps.

References

[1] M. R. Brake, P. Reuss, D. J. Segalman, L. Gaul, Variability and Repeatability of Jointed Structures with Frictional Interfaces, in: Dynamics of Coupled Structures, Volume 1, 2014, pp. 245–252 (2014).

[2] R. J. Kuether, M. R. W. Brake, Instantaneous Frequency and Damping from Transient Ring-Down Data, in: Dynamics of Coupled Structures, Volume 4, Conference Proceedings of the Society for Experimental Mechanics Series, Springer, Cham, 2016, pp. 253–263 (2016).

[3] M. S. Bonney, B. A. Robertson, M. Mignolet, F. Schempp, M. R. Brake, Experimental determination of frictional interface models, Conference Proceedings of the Society for Experimental Mechanics Series 4 (2016) 473–490 (2016). doi:10.1007/978-3-319-29763-7_47.

[4] J. Paduart, L. Lauwers, J. Swevers, K. Smolders, J. Schoukens, R. Pintelon, Identification of nonlinear systems using Polynomial Nonlinear State Space models, Automatica 46 (4) (2010) 647–656 (2010). doi:10.1016/j.automatica.2010.01.001.
URL http://dx.doi.org/10.1016/j.automatica.2010.01.001

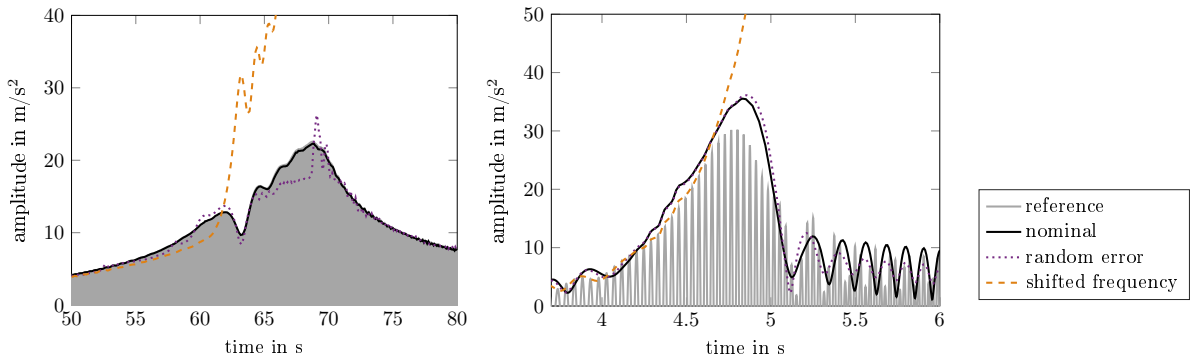

(a) (b)

Figure B.2: Predicted sweeps for (a) slow and (b) fast sweep rate. The reference is a time-simulated response based on the nominal model. The excitation force is the actual measured force with drop at resonance (see Fig. 7).

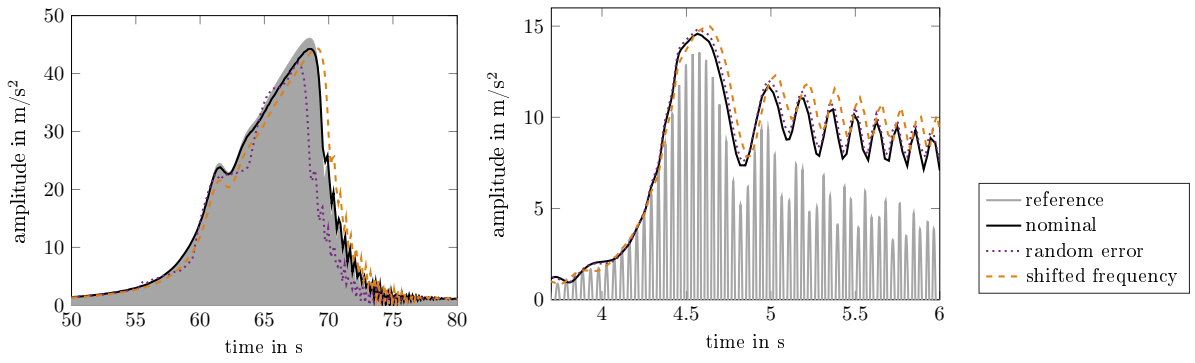

(a) (b)

Figure B.3: Predicted sweeps for (a) slow and (b) fast sweep rate. The reference is a time-simulated response based on the nominal model. The amplitude of the excitation force is constant.

[5] J. P. Noël, A. F. Esfahani, G. Kerschen, J. Schoukens, A nonlinear state-space approach to hysteresis identification, Mechanical Systems and Signal Processing 84 (2017) 171–184 (2017). doi:10.1016/j.ymssp.2016.08.025.
[6] K. Tiels, PNLSS, Vrije Universiteit Brussel, Department ELEC (2016).
[7] J. Schoukens, R. Pintelon, T. Dobrowiecki, Linear modeling in the presence of nonlinear distortions, IEEE Transactions on Instrumentation and Measurement 51 (4) (2002) 786–792 (2002). doi:10.1109/TIM.2002.803298.
[8] R. Pintelon, J. Schoukens, System identification: a frequency domain approach, 2nd Edition, IEEE Press, 2012 (2012).
[9] J. Decuyper, T. De Troyer, M. C. Runacres, K. Tiels, J. Schoukens, Nonlinear state-space modelling of the kinematics of an oscillating circular cylinder in a fluid flow, Mechanical Systems and Signal Processing 98 (2018) 209–230 (2018). doi:10.1016/j.ymssp.2017.04.048.
URL http://dx.doi.org/10.1016/j.ymssp.2017.04.048
[10] T. McKelvey, H. Akcay, L. Ljung, Multivariable System Identification From Frequency Response Data.Pdf, IEEE Transactions on Automatic Control 41 (7) (1996) 960 – 979 (1996).
[11] M. Krack, J. Gross, Harmonic Balance for Nonlinear Vibration Problems, 1st Edition, Springer International Publishing, 2019 (2019). doi:10.1007/978-3-030-14023-6.
[12] E. Gourc, C. Grappasonni, J. P. Noël, T. Detroux, G. Kerschen, Obtaining nonlinear frequency responses from broadband testing, Conference Proceedings of the Society for Experimental Mechanics Series 1 (2016) 219–227 (2016). doi:10.1007/978-3-319-29739-2_20.
[13] M. Krack, Nonlinear modal analysis of nonconservative systems: Extension of the periodic motion concept, Computers and Structures 154 (2015) 59–71 (2015). doi:10.1016/j.compstruc.2015.03.008.
URL http://dx.doi.org/10.1016/j.compstruc.2015.03.008
[14] M. Scheel, S. Peter, R. I. Leine, M. Krack, A Phase Resonance Approach for Modal Testing of Structures with Nonlinear Dissipation, Journal of Sound and Vibration submitted (2018).
[15] D. Shmilovitz, On the Definition of Total Harmonic Distortion and Its Effects on Measurement Interpretation, IEEE Transactions on Power Delivery 20 (1) (2005) 526–528 (2005).
[16] S. Peter, M. Scheel, M. Krack, R. I. Leine, Synthesis of nonlinear frequency responses with experimentally extracted nonlinear modes, Mechanical Systems and Signal Processing 101 (2018) 498–515 (2018). doi:10.1016/j.ymssp.2017.09.014.
URL http://dx.doi.org/10.1016/j.ymssp.2017.09.014
[17] M. Krack, L. Panning-Von Scheidt, J. Wallaschek, On the computation of the slow dynamics of nonlinear modes of mechanical systems, Mechanical Systems and Signal Processing 42 (1-2) (2014) 71–87 (2014). doi:10.1016/j.ymssp.2013.08.031.
URL http://dx.doi.org/10.1016/j.ymssp.2013.08.031
[18] K. W. Yung, P. B. Landecker, D. D. Villani, An Analytic Solution for the Force Between Two Magnetic Dipoles, Magnetic and Electrical Separation 9 (1) (1998) 39–52 (1998). doi:10.1155/1998/79537.
[19] G. Kleyman, S. Schwarzendahl, J. Wallaschek, Nonlinear System Identification of a Beam with Magnetic Restoring Forces, 9th European Nonlinear Dynamics Conference (ENOC 2017) (2017) 2–3 (2017).
[20] S. Mojrzisch, J. Wallaschek, J. Bremer, An Experimental Method for the Phase Controlled Frequency Response Measurement of Nonlinear Vibration Systems, in: Proceedings in Applied Mathematics and Mechanics, Vol. 12, 2012, pp. 253–254 (2012). doi:10.1002/pamm.201210117.
[21] S. Catalfamo, S. A. Smith, F. Morlock, M. R. W. Brake, P. Reuß, C. W. Schwingshackl, W. D. Zhu, Effects of Experimental Methods on the Measurements of a Nonlinear Structure, in: Dynamics of Coupled Structures, Volume 4 , Conference Proceedings of the Society for Experimental Mechanics Series, 2016, pp. 491–500 (2016).